FERMILAB-PUB-09-678-E

Measurement of Inclusive Neutral Current π^0 Production on Carbon in a Few-GeV Neutrino Beam

Y. Kurimoto,[10] J. L. Alcaraz-Aunion,[1] S. J. Brice,[4] L. Bugel,[13] J. Catala-Perez,[18] G. Cheng,[3] J. M. Conrad,[13] Z. Djurcic,[3] U. Dore,[15] D. A. Finley,[4] A. J. Franke,[3] C. Giganti,[15,*] J. J. Gomez-Cadenas,[18] P. Guzowski,[6] A. Hanson,[7] Y. Hayato,[8] K. Hiraide,[10,†] G. Jover-Manas,[1] G. Karagiorgi,[13] T. Katori,[7] Y. K. Kobayashi,[17] T. Kobilarcik,[4] H. Kubo,[10] W. C. Louis,[11] P. F. Loverre,[15] L. Ludovici,[15] K. B. M. Mahn,[3,‡] C. Mariani,[3] S. Masuike,[17] K. Matsuoka,[10] V. T. McGary,[13] W. Metcalf,[12] G. B. Mills,[11] G. Mitsuka,[9,§] Y. Miyachi,[17,¶] S. Mizugashira,[17] C. D. Moore,[4] Y. Nakajima,[10] T. Nakaya,[10] R. Napora,[14] P. Nienaber,[16] D. Orme,[10] M. Otani,[10] A. D. Russell,[4] F. Sanchez,[1] M. H. Shaevitz,[3] T.-A. Shibata,[17] M. Sorel,[18] R. J. Stefanski,[4] H. Takei,[17,**] H.-K. Tanaka,[13] M. Tanaka,[5] R. Tayloe,[7] I. J. Taylor,[6,††] R. J. Tesarek,[4] Y. Uchida,[6] R. Van de Water,[11] J. J. Walding,[6] M. O. Wascko,[6] H. B. White,[4] M. J. Wilking,[2,‡] M. Yokoyama,[10] G. P. Zeller,[11] and E. D. Zimmerman[2]

(The SciBooNE Collaboration)

[1] *Institut de Fisica d'Altes Energies, Universitat Autonoma de Barcelona, E-08193 Bellaterra (Barcelona), Spain*
[2] *Department of Physics, University of Colorado, Boulder, Colorado 80309, USA*
[3] *Department of Physics, Columbia University, New York, NY 10027, USA*
[4] *Fermi National Accelerator Laboratory; Batavia, IL 60510, USA*
[5] *High Energy Accelerator Research Organization (KEK), Tsukuba, Ibaraki 305-0801, Japan*
[6] *Department of Physics, Imperial College London, London SW7 2AZ, UK*
[7] *Department of Physics, Indiana University, Bloomington, IN 47405, USA*
[8] *Kamioka Observatory, Institute for Cosmic Ray Research, University of Tokyo, Gifu 506-1205, Japan*
[9] *Research Center for Cosmic Neutrinos, Institute for Cosmic Ray Research, University of Tokyo, Kashiwa, Chiba 277-8582, Japan*
[10] *Department of Physics, Kyoto University, Kyoto 606-8502, Japan*
[11] *Los Alamos National Laboratory; Los Alamos, NM 87545, USA*
[12] *Department of Physics and Astronomy, Louisiana State University, Baton Rouge, LA 70803, USA*
[13] *Department of Physics, Massachusetts Institute of Technology, Cambridge, MA 02139, USA*
[14] *Department of Chemistry and Physics, Purdue University Calumet, Hammond, IN 46323, USA*
[15] *Università di Roma La Sapienza, Dipartimento di Fisica and INFN, I-00185 Rome, Italy*
[16] *Physics Department, Saint Mary's University of Minnesota, Winona, MN 55987, USA*
[17] *Department of Physics, Tokyo Institute of Technology, Tokyo 152-8551, Japan*
[18] *Instituto de Fisica Corpuscular, Universidad de Valencia and CSIC, E-46071 Valencia, Spain*

(Dated: February 5, 2010)

The SciBooNE Collaboration reports inclusive neutral current neutral pion production by a muon neutrino beam on a polystyrene target (C_8H_8). We obtain $(7.7 \pm 0.5(\text{stat.}) \pm 0.5(\text{sys.})) \times 10^{-2}$ as the ratio of the neutral current neutral pion production to total charged current cross section; the mean energy of neutrinos producing detected neutral pions is 1.1 GeV. The result agrees with the Rein-Sehgal model implemented in our neutrino interaction simulation program with nuclear effects. The spectrum shape of the π^0 momentum and angle agree with the model. We also measure the ratio of the neutral current coherent pion production to total charged current cross section to be $(0.7 \pm 0.4) \times 10^{-2}$.

PACS numbers: 13.15.+g, 13.60.Le, 25.30.Pt, 95.55.Vj

arXiv:0910.5768v3 [hep-ex] 5 Feb 2010

*Present address: DSM/Irfu/SPP, CEA Saclay, F-91191 Gif-sur-Yvette, France
†Present address: Kamioka Observatory, Institute for Cosmic Ray Research, University of Tokyo, Gifu 506-1205, Japan
‡Present address: TRIUMF, Vancouver, British Columbia, V6T 2A3, Canada
§Present address: Solar-Terrestrial Environment Laboratory, Nagoya University, Furo-cho, Chikusa-ku, Nagoya, Japan
¶Present address: Department of Physics, Yamagata University, Yamagata, 990-8560 Japan
**Present address: Kitasato University, Tokyo, 108-8641 Japan
††Present address: Department of Physics and Astronomy, State University of New York, Stony Brook, NY 11794-3800, USA

I. INTRODUCTION

Neutrino-nucleus cross sections have been intensively studied for decades. However, the precision and understanding of the cross sections around 1 GeV are still not satisfactory. The next generation of neutrino oscillation experiments will search for sub-leading flavor oscillation and charge-parity symmetry violation; the precision needed for these searches drives the need for more accurate independent measurements of neutrino cross sections [1, 2]. Although several interaction channels contribute to the total neutrino-nucleus cross section in the neutrino energy range of a few GeV, an understanding of neutral current neutral pion production (NCπ^0) is especially important. NCπ^0 events form the largest ν_μ-induced background to neutrino experiments measuring $\nu_\mu \to \nu_e$ oscillations in the neutrino energy range of a few GeV or less, such as the T2K experiment [1]. NCπ^0 events can mimic ν_e signal events when, for example, one of the two photons associated with $\pi^0 \to \gamma\gamma$ is not detected.

NCπ^0production has been measured by several past experiments [3–7]. However, their results have large uncertainty due to low statistics and are not useful expressions for predicting electron backgrounds in $\nu_\mu \to \nu_e$ oscillation searches, since they are typically given as ratios to the charged current (CC) single pion production cross section, which is also poorly known. T2K [1] uses a neutrino beam whose mean neutrino energy is approximately 0.8 GeV. The experiment requires less than a 10% uncertainty on NCπ^0 production to maintain high sensitivity for the $\nu_\mu \to \nu_e$ oscillation search. Recently, two experiments published NC π^0 production results. The K2K collaboration reported NC π^0 production in water with a 1.3 GeV mean neutrino energy beam[8], finding their measurement consistent with the Monte Carlo (MC) prediction based on the Rein and Sehgal model [9]. MiniBooNE reported the yield and spectral shape of π^0 s as a function of π^0 momentum and the observation of NC coherent π^0 production in mineral oil (CH_2) in neutrino beam of mean neutrino energy 0.7 GeV [10]. The total NCπ^0 cross section below 1 GeV has still not been precisely measured yet.

Pions are produced mainly through two distinct mechanisms by neutrinos with energies around 1 GeV. In the dominant mode, resonant pion production, the neutrino interacts with a nucleon in the nucleus and excites it to a baryonic resonance, such as Δ (1232), which subsequently decays to a pion and a nucleon. The other mode, coherent pion production occurs when the neutrino interacts with the target nucleus so that no nuclear breakup occurs. Resonance production and decay in a nuclear target differs from the case of the free nucleon target. This is due to nuclear effects such as Fermi motion, Pauli blocking, and the nuclear potential. In addition, produced mesons and baryons interact with nuclear matter until they escape from the target nucleus. Due to this final state interaction, the number, momenta, directions and charge states of produced particles can be changed in nuclear matter. Although there are several theoretical models of these processes, their uncertainties are still large. To understand the production mechanism and the nuclear effects, measurements of emitted π^0 kinematics are very important.

Recent measurements of coherent pion production have drawn much attention. For CC coherent pion production, the K2K experiment placed a limit on the ratio of the CC coherent pion production to the total CC cross sections at 1.3 GeV[11]. This result was confirmed by the SciBooNE experiment [12], although recent data from the SciBooNE collaboration suggest CC coherent pion production at a level below the published limit in both neutrinos and antineutrinos [13, 14]. Moreover, evidence for NC coherent pion production with neutrino energy less than 2 GeV has been reported by the MiniBooNE Collaboration [10]. Hence, it is interesting to search for NC coherent π^0 production in the SciBooNE data.

In this paper, we present measurements of the NCπ^0 interaction in polystyrene (C_8H_8) using the same neutrino beam as MiniBooNE (with mean neutrino energy 0.7 GeV). We measure the ratio of the total inclusive NCπ^0 cross section to the total CC cross section and kinematic distributions of the emitted π^0s. We also extract the fraction of coherent NC π^0 events from the inclusive NC π^0 data sample. In these analyses, we define NCπ^0 events to be NC neutrino interactions with at least one π^0 emitted in the final state from the target nucleus.

II. EXPERIMENT DESCRIPTION

A. Neutrino Beam

The SciBooNE experiment detected neutrinos produced by the Fermilab Booster Neutrino Beam (BNB). The same BNB beam is also serving the MiniBooNE experiment. The BNB uses protons accelerated to 8 GeV kinetic energy by the Fermilab Booster synchrotron. Beam properties are monitored on a spill-by-spill basis, and at various locations along the BNB line. Transverse and directional alignment of the beam, beam width and angular divergence, beam intensity and losses along the BNB, are measured and used to monitor data quality. Protons strike a 71.1 cm long beryllium target, producing a secondary beam of hadrons, mainly pions with a small fraction of kaons. A cylindrical horn electromagnet made of aluminum surrounds the beryllium target to sign-select and focus the secondary beam. For the data set used in this measurement, the horn polarity was set to neutrino mode, focusing (defocusing) particles with positive (negative) electric charge. The neutrino beam is mostly produced in the 50 m long decay region, mainly from $\pi^+ \to \mu^+\nu_\mu$ in-flight decays. See [15] for further details.

B. Neutrino Detector

The SciBooNE detector was located 100 m downstream from the beryllium target on the axis of the beam. The detector comprised three sub-detectors: a fully active and finely segmented scintillator tracker (SciBar), an electromagnetic calorimeter (EC), and a muon range detector (MRD). SciBar served as the primary neutrino target for this analysis.

Fig. 1 shows an event display of a typical NCπ^0 production event candidate. SciBooNE uses a right-handed Cartesian coordinate system in which the z axis is the beam direction and the y axis is the vertical upward direction. The origin is located on the most upstream surface of SciBar in the z dimension, and at the center of the SciBar scintillator plane in the x and y dimensions. Since each sub-detector is read out both vertically and horizontally, two views are defined: top (x *vs.* z projection) and side (y *vs.* z projection).

The SciBar detector [16] was positioned upstream of the other sub-detectors. It consists of 14,336 extruded plastic scintillator strips which serve as the target for the neutrino beam as well as the active detection medium. Each strip has a dimension of $1.3 \times 2.5 \times 300$ cm^3. The scintillators are arranged vertically and horizontally to construct a $3 \times 3 \times 1.7$ m^3 volume with a total mass of 15 tons. SciBar has about four radiation lengths of material along the beam direction. Each strip was read out by a wavelength shifting (WLS) fiber attached to a 64-channel multi-anode PMT. Charge information was recorded for each channel, while timing information was recorded in groups of 32 channels by taking the logical OR with multi-hit TDC modules [17].

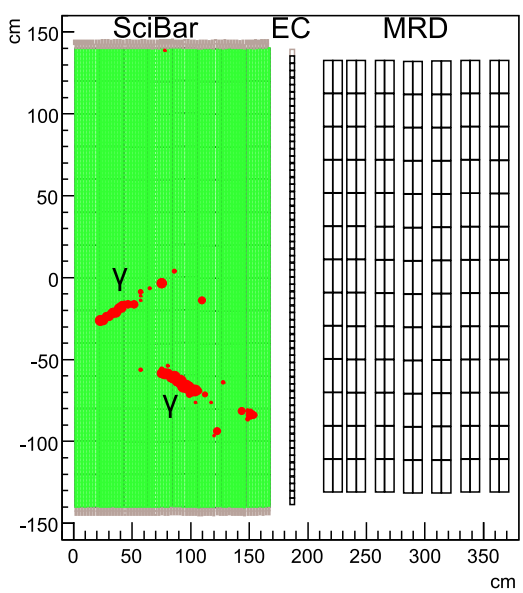

FIG. 1. Event display of a typical NCπ^0 event candidate in SciBooNE data. The neutrino beam runs from left to right in this figure, encountering SciBar, the EC and MRD, in that order. The circles on SciBar indicate ADC hits for which the area of the circle is proportional to the energy deposition in that channel. This event display shows the electromagnetic shower tracks from the pair conversions of the two π^0 decay photons.

The gains of all PMT channels, attenuation of WLS-fibers, and light yield of each scintillator were continuously monitored *in situ* using LED and cosmic ray data taken between beam spills, with precision better than 1%. The timing resolution for minimum-ionizing particles was evaluated with cosmic ray data to be 1.6 ns. The average light yield for minimum-ionizing particles is approximately 20 photoelectrons per 1.3 cm path length, and the typical pedestal width is below 0.3 photoelectron. The hit finding efficiency evaluated with cosmic ray data is more than 99.8%. The minimum length of a reconstructable track is approximately 8 cm (three layers hit in each view). The track finding efficiency for single tracks of 10 cm or longer is more than 99%.

The EC is located just downstream of SciBar, and is designed to measure the electron neutrino contamination in the beam and tag photons from π^0 decay. The EC is a "spaghetti" type calorimeter comprised of 1 mm diameter scintillating fibers embedded in lead foil [18]. The calorimeter is made of 64 modules of dimensions $262 \times 8 \times 4$ cm^3. The fibers are bundled in two independent groups of 4×4 cm^2 transverse cross section, read at both ends by Hamamatsu PMTs. The EC comprises one vertical and one horizontal plane (32 modules each), covering an active area of 2.65×2.65 m^2. The EC has a thickness of 11 radiation lengths along the beam direction. The charge information from each PMT was recorded. A minimum ionizing particle with a minimal path length deposits approximately 91 MeV in the EC. The energy resolution for electrons was measured to be $14\%/\sqrt{E\ (\mathrm{GeV})}$ using a test beam [18]. The detection efficiency for cosmic muons is 96%; the inefficiency stems from gaps between the modules.

The MRD was installed downstream of the EC and is designed to measure the momentum of muons produced by CC neutrino interactions. It had 12 iron plates with thickness 5 cm sandwiched between planes of 6 mm thick scintillation counters; there were 13 alternating horizontal and vertical planes read out via 362 individual 2 inch PMTs. Each iron plate measured 274×305 cm^2. The MRD measured the momentum of muons up to 1.2 GeV/c using the observed muon range. Charge and timing information from each PMT were recorded. Hit finding efficiency was continuously monitored using cosmic ray data taken between beam spills; the average hit finding efficiency is 99%.

C. Data Summary

The SciBooNE experiment took data from June 2007 until August 2008. After applying data quality cuts to all beam events[12], 2.52×10^{20} protons on target are usable for physics analysis, with 0.99×10^{20} protons on target collected in neutrino mode. The analysis presented herein uses only neutrino mode data.

III. EXPERIMENT SIMULATIONS

A. Neutrino Flux Prediction

Predictions for the BNB neutrino flux illuminating the SciBooNE detector are obtained via a GEANT4 simulation of the beamline. The simulation accounts for all relevant beamline geometry and materials, the measured BNB beam optics properties, and the horn magnetic field. Hadronic interactions are carefully modeled. Cross sections for elastic, quasi-elastic and other inelastic interactions of charged pions and nucleons with beryllium and aluminum are simulated according to a custom model validated with external data, and covering the most relevant momentum range (down to 0.5 GeV/c for pions, 2 GeV/c for nucleons). Furthermore, the multiplicity and kinematics of all relevant particle types produced in the inelastic interactions of primary (8.4-8.9 GeV/c) protons with beryllium are also described by a custom model based on external data. For π^+ production, a parameterization based on HARP [19] and BNL E910 [20] data is used. Other hadronic and all electromagnetic processes of importance to neutrino production are described instead by standard GEANT4 models. The modeling of neutrino-producing weak decays incorporates accurate knowledge of meson decay branching fractions and form factors, and includes muon polarization effects. For a detailed description of the BNB simulation code, see [15]. According to the simulation, the neutrino flux at the SciBooNE detector is dominated by muon neutrinos (93%), while the neutrino energy spectrum peaks at $\sim$ 0.6 GeV, has a mean neutrino energy of $\sim$ 0.7 GeV, and extends up to 2-3 GeV [12].

B. Neutrino Interaction Simulation

In the SciBooNE experiment, neutrino interactions with nuclear targets are simulated by the NEUT program library [21, 22] that is used in the Kamiokande, Super-Kamiokande, K2K, and T2K experiments.

The nuclear targets handled in NEUT are protons, carbon, oxygen, and iron. The energy of neutrinos handled by the simulation ranges from 100 MeV to 100 TeV. The types of neutrino interactions simulated in both NC and CC are : elastic and quasi-elastic scattering ($\nu N \to \ell N'$), single meson production ($\nu N \to \ell N' m$), single gamma production ($\nu N \to \ell N' \gamma$), coherent π production (ν^{12}C(or^{56}Fe) $\to \ell\pi$ ^{12}C(or^{56}Fe)), and deep inelastic scattering ($\nu N \to \ell N' hadrons$), where N and N' are the nucleons (proton or neutron), ℓ is the lepton (electron, muon or neutrino), and m is the meson. In nuclei, interactions of the mesons and hadrons with the nuclear medium are simulated following the neutrino interactions.

1. *Single meson production via baryon resonances*

The main signal in this analysis is NC single π^0 production via baryon resonances. The resonant single meson production is simulated based on the model of Rein and Sehgal [9]. The cross section of the NC single π^0 production per nucleon on a polystyrene target (C_8H_8) in NEUT is shown in Fig. 2. The per nucleon cross section of a CH molecule is calculated by summing the contributions from the six protons and six neutrons bound in the carbon nucleus as well as the free proton, and dividing that by 13. Following production, the intra-nuclear interactions of the meson and nucleons are simulated using a cascade model in which the particles are traced until escaping from the nucleus. According to this model, approximately 40% of π^0s interact in the target nucleus, averaged over our neutrino flux. For scattering off nucleons in the nucleus by a neutrino, the relativistic Fermi gas model of Smith and Moniz [23] is implemented. The nucleons are treated as quasi-free particles and the Fermi motion of nucleons along with the Pauli exclusion principle is taken into account. The Fermi surface momentum is set to 217 MeV/c and the nuclear potential is set to 27 MeV for carbon. The vector and axial-vector form factors are formalized to be dipole with $M_V^{1\pi} = 0.84$ GeV/c^2 and $M_A^{1\pi} = 1.21$ GeV/c^2. The same Fermi momentum distribution, nuclear potential and Q^2-dependence of form factors are used in all other neutrino-nucleus interactions except for coherent π production.

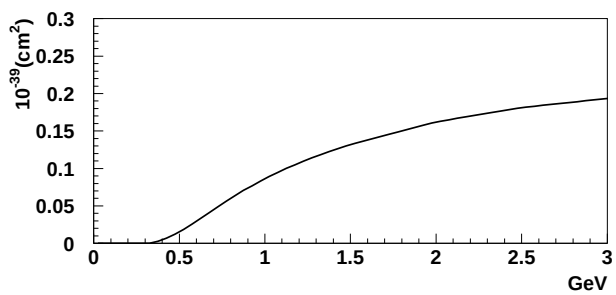

FIG. 2. Cross section versus neutrino energy of NC single π^0 production per nucleon on a polystyrene target (C_8H_8) estimated in NEUT; the curve is based on the Rein and Sehgal model.

The Rein and Sehgal model assumes an intermediate baryon resonance, N^*, in the reaction of $\nu N \to \ell N^*, N^* \to N' m$. All intermediate baryon resonances

with mass less than 2 GeV/c^2 are included. Baryon resonances with mass greater than 2 GeV/c^2 are simulated as deep inelastic scattering. Pion-less Δ decays—which produce no pion in the final state and account for 20% of Δ events [24]—are also simulated. To determine the angular distribution of final state pions, Rein's method [25] is used for the $P_{33}(1232)$ resonance. For other resonances, the directional distribution of the generated pion is chosen to be isotropic in the resonance rest frame.

The inelastic scattering, charge exchange and absorption of pions in nuclei are simulated. The interaction cross sections of pions in the nuclei are based on the model by Salcedo *et al.* [26]. For inelastic scattering and charge exchange interactions, the direction and momentum of pions are affected. In the scattering amplitude, Pauli blocking is also taken into account.

2. *Coherent π production*

The π^0 signal events contain a contribution from NC coherent π^0 production. Due to the small momentum transfer to the target nucleus, the outgoing neutrino and the pion tend to go in the forward direction. The formalism developed by Rein and Sehgal [27, 28] is used to simulate the interactions. The axial vector mass, $M_A^{coherent}$, is set to 1.0 GeV/c^2, and the nuclear radius parameter R_0 is set to 1.0 fm. For the total and inelastic pion-nucleon cross sections used in the formalism, the fitted results given in Rein and Sehgal's paper are employed. The NC coherent π^0 production cross section on a polystyrene target is shown in Fig. 3, with the NC single π^0 production via baryon resonances and the total CC cross sections. The Rein and Sehgal model predicts the NC coherent π^0 production rate to be approximately 1% of the total neutrino CC rate in SciBooNE.

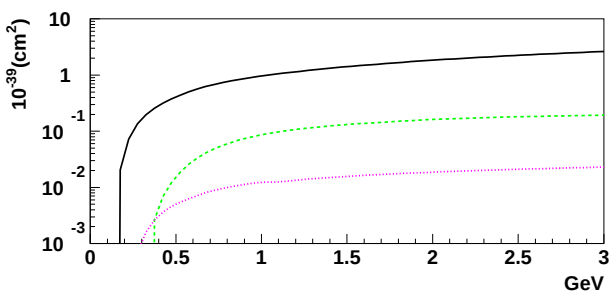

FIG. 3. Cross sections versus neutrino energy of the total CC interaction (solid line), the NC single π^0 production via baryon resonances (dashed line) and the NC coherent π^0 production (dotted line) calculated in NEUT per nucleon on polystyrene target.

TABLE I. The expected number and fraction of events in each neutrino interaction estimated by NEUT at the SciBooNE detector location with the neutrino beam exposure of 0.99×10^{20} protons on target. The 10.6 ton fiducial volume of the SciBar detector is assumed. CC and NC interactions are abbreviated as CC and NC, respectively.

Interaction Type	# Events	Fraction(%)
CC quasi-elastic	53,363	41.4
CC single π via resonances	29,688	23.1
CC coherent π	1,771	1.4
CC single meson except π	839	0.7
CC DIS	6,074	4.7
NC elastic	22,521	17.5
NC single π^0 via resonances	6,939	5.4
NC coherent π^0	1,109	0.9
NC single meson except π^0	4,716	3.7
NC DIS	1,768	1.4

3. *Quasi-elastic scattering and deep inelastic scattering*

The dominant interaction in the SciBooNE neutrino energy is CC quasi-elastic scattering, which is implemented using the Smith and Moniz model [23]. M_V^{QE} and M_A^{QE} are set to be 0.84 GeV/c^2 and 1.21 GeV/c^2, respectively.

The deep inelastic scattering (DIS) cross section is calculated using the GRV98 parton distribution functions [29]. As well as quasi-elastic scattering and deep inelastic scattering, other neutrino interactions in NEUT are described in [12] in detail.

With the SciBooNE neutrino beam exposure of 0.99×10^{20} protons on target, the expected number of events in the SciBooNE detector in each neutrino interaction is listed in Tab. I. For the purpose of systematic studies of neutrino interaction simulations, we also use the NUANCE event generator [30] that is used in the MiniBooNE experiment. The types and models of neutrino interactions in NUANCE are similar to those of NEUT but with different treatment of re-interactions of mesons and hadrons with the nuclear medium.

C. Neutrino detector simulation

The GEANT4 framework is used for the detector simulation. The Bertini cascade model within GEANT4 [31] is used to simulate the interactions of hadronic particles with detector materials. The detector simulation includes a detailed geometric model of the detector, including the detector frame and experimental hall and soil, based on survey measurements taken during detector construction. A description of the detector simulation is given in [12].

In addition to neutrino interactions inside the detector, we also simulate interactions in the surrounding material

(the walls of the detector hall and soil). The density of material is assumed to be 2.15 g/cm^3 for the calculation of the interaction rate, and concrete of that density is used as the material for propagation of product particles. We generate events in a volume of ±5 m in x, y, and z direction in the SciBooNE coordinates.

IV. DATA ANALYSIS

The present analysis has two main goals. The first is to measure the ratio of NCπ^0 production cross section to the total CC cross section. We measure the ratio of cross sections in order to minimize systematic uncertainty due to the neutrino flux prediction. The second goal is to measure the π^0 momentum and angular spectra. In addition to the two main goals, we also extract the coherent π^0 fraction in the context of the Rein and Sehgal model.

We reconstruct gamma rays converting in SciBar and select events with two reconstructed gamma rays and no muons, which is the characteristic topology of NCπ^0events. We do not include NCπ^0events in which one or both gamma rays convert in the EC.

A. Signal Definition

We define an NCπ^0 interaction as an NC neutrino interaction in which at least one π^0 is emitted in the final state from the target nucleus, $\nu_\mu C \rightarrow \nu_\mu \pi^0 X$ where X represents the nuclear remnant and any combination of nucleons and mesons. According to our MC simulation, 96% of NCπ^0 events without any selection cuts have a single π^0 (85% from a single π^0 without any other mesons and 11% from a single π^0 with charged mesons) and 4% have two π^0s. Any π^0 emitted from the initial target nucleus constitutes a signal event whether it is created from the neutrino vertex or final state interactions. Events with a π^0 produced in the neutrino interaction but absorbed in the target nucleus are not included in the signal sample, nor are events in which π^0s are produced by secondary particles interacting with the detector scintillator outside the target nucleus.

B. Gamma Ray Reconstruction

1. Gamma Conversion Probability

Since the length of SciBar in the beam direction corresponds to four radiation lengths, a significant fraction of gamma rays escape from SciBar without conversion. In 30% of events with a π^0 emitted within SciBar's fiducial volume, both gamma rays convert in SciBar; in 38%, only one gamma ray converts in SciBar; in 32%, neither gamma ray converts in SciBar. Since we aim to reconstruct two gamma rays to identify NCπ^0 events, the maximum detection efficiency attainable is 30%.

2. Track Reconstruction

The first step of the event reconstruction is to search for two-dimensional tracks in each view of SciBar using a cellular automaton algorithm [32]. For tracking, the hit threshold is set to 2.5 photo-electrons, corresponding to roughly 0.25 MeV. Three dimensional tracks are reconstructed by matching the timing and z-edges of the two dimensional projections. In order to match track projections in a three dimensional track, the timing difference between two two-dimensional projections is required to be less than 50 ns, and the z-edge difference must be less than 6.6 cm for upstream and downstream edges. This method is used for all charged particles and is the first step of gamma ray reconstruction.

3. Particle Identification Parameter

The SciBar detector has the capability to distinguish protons from other particles using dE/dx since recoil protons at SciBooNE energies interact well above minimum ionizing energy deposit. We define a muon confidence level (MuCL) using the observed energy deposit per layer for all reconstructed tracks[12]. The MuCL of the proton tracks tends to be close to 0 while the MuCL of other tracks tends to be close to 1. Proton-like tracks are defined to have MuCL less than 0.03.

4. Extended Track

Single reconstructed tracks are extended in two ways to improve the energy reconstruction of gamma rays within SciBar. The first step is merging two or more tracks if they are nearly co-linear, because electromagnetic showers can form separate hit clusters in SciBar resulting in two or more tracks. The second step is collecting lone hits around merged tracks. Electromagnetic showers sometimes deposit energy around the main track and these hits are missed by the track reconstruction algorithm. Hits not assigned to any track within 20 cm from 2D projections of the merged track (*i.e.*, after the first step) for each view are added to the extended track. The methods described above are applied only to non-proton-like tracks. For the energy reconstruction, we use charge information of hits associated with original tracks as well as newly assigned hits. For reconstructing the directions of gamma rays, we fit positions of hits in all original tracks in the extended track with a straight line and do not use hits newly collected in the second step.

5. SciBar-EC matching

Gamma rays can escape SciBar to deposit energy in the EC. After event reconstruction in SciBar, we search for EC clusters aligned with tracks from SciBar. One EC

cluster is defined as a collection of neighboring EC hits. For an EC hit, the pulse heights of both side PMTs are required to be above threshold, which is set to 3 times the width of each pedestal—about 7 MeV. The energy of an EC hit is the geometric average of the two PMTs. The center of an EC cluster is defined as the energy-weighted average of hits in the cluster. To match an EC cluster to an SciBar track, the EC cluster is required to be within 10 cm of the extrapolated two-dimensional projections of the SciBar track in each EC plane. The energy of matched EC clusters is added to the corresponding extended tracks.

6. *Gamma Ray Reconstruction Performance*

We study the performance of the gamma ray reconstruction algorithms using the MC simulation. The angular resolution of gamma rays passing all selection cuts (see section IV D) is estimated to be approximately 6°. For the energy reconstruction, energy of matched EC clusters is added to corresponding extended tracks. About 7% of selected extended tracks are made by two or more tracks. The average gamma ray energy deposit of SciBar is estimated to be 116 MeV and the energy resolution is estimated to be 6%. About 17% of selected extended tracks have matched EC clusters. The average gamma ray energy deposit in such matched EC clusters is estimated to be 72 MeV and the energy resolution is estimated to be 32%.

Not all gamma ray energy is deposited in, nor recorded by, the detector. Such lost energy is called leakage. The actual leakage, defined as

$$L_{act} = 1 - \frac{\text{gamma energy in extended track}}{\text{true gamma energy}}, \quad (1)$$

is estimated to be 24%; 11% comes from energy loss in passive regions and gamma rays escaping from the detectors and 13% comes from energy deposit in active regions but not assigned to the extended track. The reconstructed energy can include energy deposited by other particles. On average, 15% of the total energy in an extended track comes from other particles. Due to this contamination, the effective leakage, defined as:

$$L_{eff} = 1 - \frac{\text{reconstructed energy of extended track}}{\text{true gamma energy}} \quad (2)$$

is 15%, which is smaller than L_{act} averaged over all NCπ^0 events.

C. CC Event Selection

To identify CC events, we search for events in which at least one reconstructed track in SciBar, when projected out of SciBar, is matched with a track or hits in the MRD. We reject events with hits associated with the muon track on the most upstream layer of SciBar to eliminate neutrino-induced incoming particles from the upstream wall or soil. The neutrino interaction vertex for CC events is reconstructed as the upstream edge of the muon track. We select events whose vertices are in the SciBar fiducial volume, defined to be ±130 cm in both the x and y dimensions, and 2.62 cm$< z <$157.2 cm, a fiducial mass of 10.6 tons. The time of the muon track is required to be within a 2 μs window around the beam pulse. Finally, we require the muon track to stop in the MRD. The MRD-stopped event sample [12] serves as the normalization sample in the cross-section ratio measurement. Unless otherwise indicated, the MC distributions in this paper are normalized using the MRD-stopped data sample.

D. NCπ^0 Event Selection

The clearest feature of NC π^0 production is two gamma rays, coming from the decay of the π^0, converted into two e^+e^- pairs. Background events stem from sources both internal and external to SciBar. Internal backgrounds are neutrino interactions other than NCπ^0(mainly CC) within SciBar; external backgrounds come from neutrino interactions in the material outside of the detector volume (support structure, walls and soil—so called dirt events) as well as from cosmic rays. In dirt events, neutrinos interact with materials such as the walls of the experimental hall or soil and produce secondary particles which deposit energy within SciBar's fiducial volume and cause recorded hits. The contribution of accidental cosmic rays in any event sample is small and accurately estimated by data taken with off-beam timing; the fraction of accidental cosmic ray events is 1.8% after all event selection cuts. Data distributions shown hereafter have been cosmic-ray subtracted from them. The event selection cuts for NCπ^0 production are developed to select events with two gamma rays while rejecting these backgrounds.

1. *Pre-selection Cuts*

We select events with at least two three-dimensional tracks. The timing of tracks are required to be within 50 ns of each other and the closest endpoints of any two tracks are required to be in the fiducial volume defined in Sec. IV D. The closest endpoints are chosen as the edge combination for two given tracks that gives the minimum distance among the four possible combinations. The times of the two tracks are required to be within the 2 μs beam window. In addition, we reject events with hits in the first layer of SciBar within 100 ns from the times of tracks, to remove dirt background events.

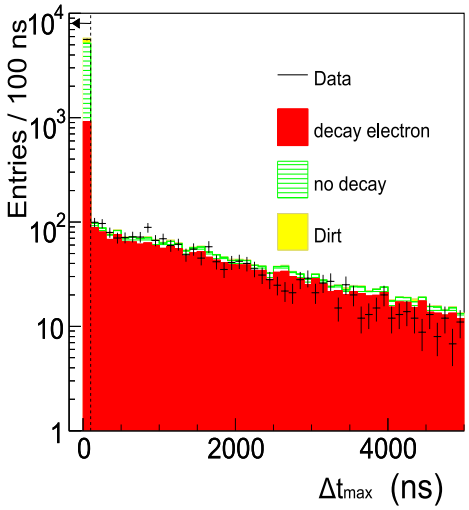

FIG. 4. $\Delta t_{\max}$ distribution (IV D 2) after rejection of side escaping tracks. The contributions from events with decay electrons, events without decay electrons and the dirt events are shown separately for the MC simulation.

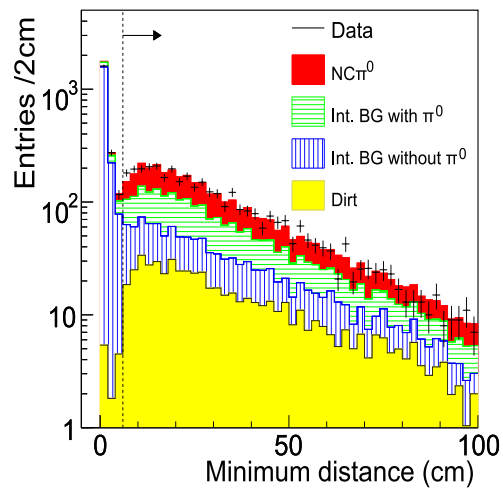

FIG. 5. The minimum distance between two tracks after muon rejection cuts. The contribution from NCπ^0 production, internal backgrounds with a π^0 in the final state, internal background without a π^0 in the final state and "dirt" background events are shown separately for the MC simulation.

2. *Muon Track Rejection Cuts*

Events with muons are predominantly CC events. To avoid muons which escape SciBar but do not penetrate the MRD, we reject events with tracks escaping from the side of SciBar; both edges of tracks must be in ± 130 cm in both the x and y dimensions.

To reject muons stopping in SciBar, we tag the electrons from muon decay. No charge information is recorded for any scintillator strip after its first hit in an event, but the times of hits above threshold continue to be recorded. Thus most decay electrons are not reconstructed as tracks but can be identified as delayed time hits near the end of a muon track. We examine the maximum timing difference ($\Delta t_{\max}$) between the track times and late hits times at the ends of tracks. Events with decay electrons yield high values of $\Delta t_{\max}$ because of the long muon lifetime ($\tau_\mu = 2.2\ \mu$ sec). Figure 4 shows the $\Delta t_{\max}$ distribution. We select events with $\Delta t_{\max}$ less than 100 ns.

3. *Track Disconnection Cut*

CC events often have two or more tracks with a common vertex while two gamma rays from π^0s are typically isolated from each other. Hence, the distance between two tracks is used to separate two gamma rays from CC events. If there are two particles with a common vertex, the minimum distance is close to zero. Figure 5 shows the distribution of the minimum distance. Events with a minimum distance greater than 6 cm are selected.

4. *Electron Catcher Cut*

Matched EC Clusters are used to reject muons penetrating the EC. Two quantities are used: the energy deposit in matched EC clusters in the upstream layer, E_1 (E_2 is energy in the downstream layer), and the ratio of energy deposits in the downstream EC cluster over the upstream EC cluster, $\mathrm{R_{EC}} = E_2/E_1$. Figure 6, 7 and 8 shows the distributions of the number of tracks with matched EC clusters, E_1 and $\mathrm{R_{EC}}$, respectively. Events satisfying one of the three following condition are selected, (i) No matched EC clusters or (ii) $E_1 > 150$ MeV or (iii) $\mathrm{R_{EC}} < 0.2$. For events without matched EC clusters, both E_1 and $\mathrm{R_{EC}}$ are left undefined (not included in Fig. 7 and 8). For events with only upstream matched EC clusters, the minimum E_1 is chosen and $\mathrm{R_{EC}}$ is set to 0. For events with both upstream and downstream matched EC clusters, the maximum $\mathrm{R_{EC}}$ is chosen and the corresponding E_1 is chosen.

5. *Number of Photon Tracks*

We use the extended track information instead of the track information hereafter. As described in Sec.IV B 4, we only use non-proton-like tracks to obtain extended tracks. Fig. 9 shows the MuCL distribution after the EC cut. The dashed line (MuCL = 0.03) separates into particles to proton-like or non-proton-like tracks. The gamma ray efficiency for the non-proton-like sample is 87% and the contamination of gamma rays in the non-

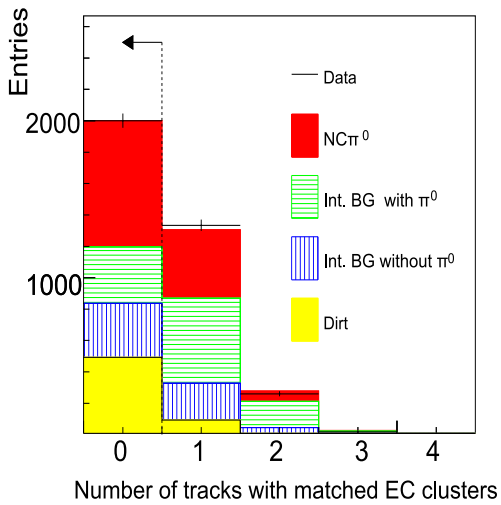

FIG. 6. Option 1 of the EC cut: the number of track with matched EC clusters after the track disconnection cut. Events without SciBar-EC matched tracks pass the EC cut. Events with SciBar tracks matching EC clusters can pass the EC cut if they satisfy the requirement shown in Fig. 7 or 8

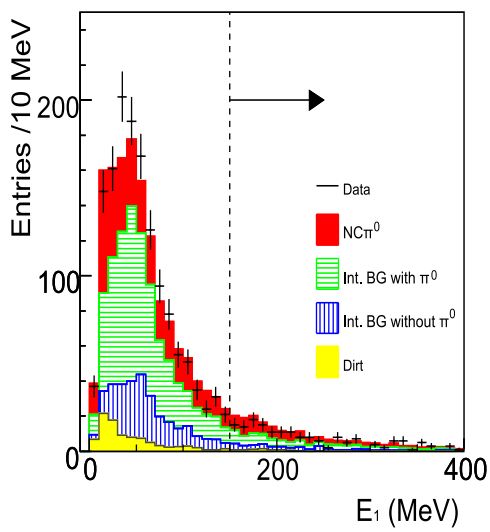

FIG. 7. Option 2 of the EC cut: the energy deposited in the upstream layer of the EC (E_1) after the track disconnection cut. Events with $E_1 > 150$ MeV pass the EC cut. Events with $E_1 < 150$ MeV can pass the EC cut if they satisfy the requirement shown in Fig. 8

proton-like sample is 81%.

Figure 10 shows the distribution of the number of extended tracks after the EC cut. To reconstruct π^0s, events with more than one extended track are selected. As shown in Fig. 10, 58% of the NCπ^0 events have only one extended track and are rejected by this cut. However, 39% are events with one reconstructed gamma ray,

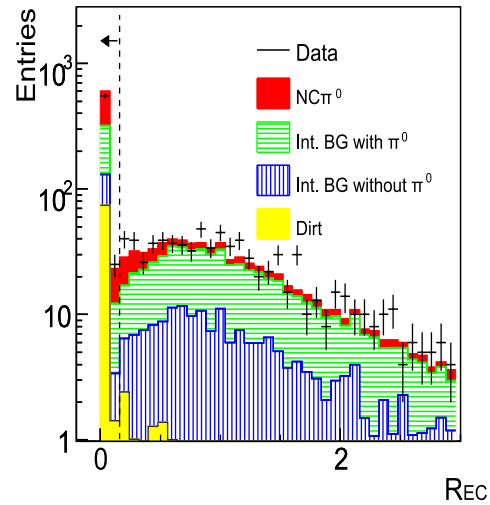

FIG. 8. Option 3 of the EC cut: the ratio of deposited energy in the downstream over the upstream layer (R) after the track disconnection cut. Only events with $E_1 < 150$ MeV are shown.

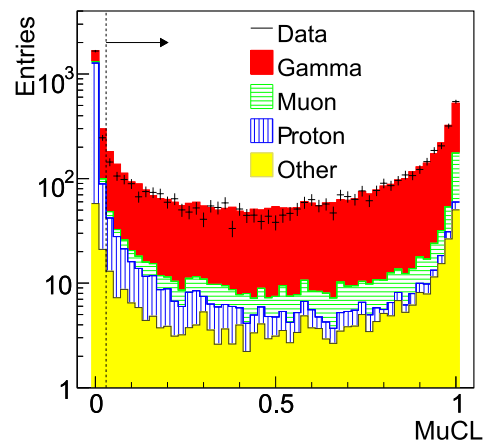

FIG. 9. The muon confidence level (MuCL) of tracks after the EC cut. The contributions from true gamma ray, muon, and proton tracks are shown separately for the MC simulation.

due to mis-reconstruction or gamma rays not converting in SciBar. Such events can not be used for π^0 reconstruction; 12% are events where the two gamma rays are reconstructed as two tracks but one of them is identified as a proton-like track; 7% are events in which the two gamma rays are reconstructed as two tracks but then merged, resulting in one extended track.

This cut is also effective at rejecting dirt backgrounds since many dirt background events have only one extended track, as shown in Fig. 10.

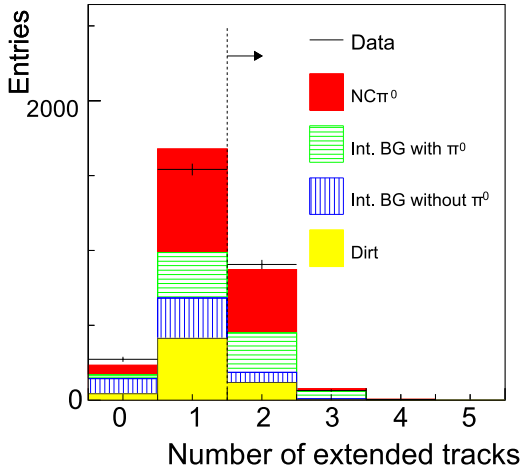

FIG. 10. The distribution of the number of extended tracks after the EC cut.

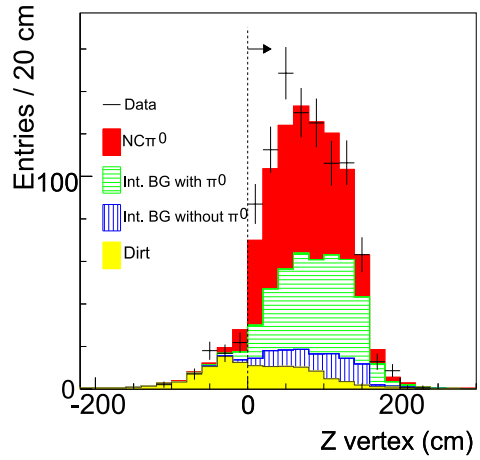

FIG. 11. The reconstructed z-vertices of π^0s after the requirement of at least two extended tracks.

6. *Reconstructed π^0 Vertex Position Cut*

The reconstructed vertex position of a π^0 is calculated as the intersection of two two-dimensional extended tracks. First, we calculate the intersection point for all combinations of extended tracks in each view—two z positions ($z_{\rm top}$ and $z_{\rm side}$) for each combination. We choose the combination giving the minimum $|z_{\rm top} - z_{\rm side}|$ as the π^0 candidate. The reconstructed z-vertices are obtained by taking the error weighted average of $z_{\rm top}$ and $z_{\rm side}$:

$$z = \frac{\frac{z_{top}}{\delta z_{top}{}^2} + \frac{z_{side}}{\delta z_{side}{}^2}}{\frac{1}{\delta z_{top}{}^2} + \frac{1}{\delta z_{side}{}^2}}, \qquad (3)$$

where $\delta z_{top(side)}$ is the error on $z_{\rm top(side)}$ returned by the track reconstruction algorithm. Figure 11 shows the reconstructed z-vertices of π^0s. The vertex resolution is approximately 12 cm for all three dimensions. Most events with a π^0 produced in SciBar yield a vertex within SciBar—but many dirt events yield a vertex position upstream of SciBar—so we select events with reconstructed π^0 z-vertex greater than 0 cm.

7. *Reconstructed π^0 Mass*

Figure 12 shows the reconstructed mass of the π^0 calculated as $\sqrt{2\mathrm{E}^{\rm rec}_{\gamma 1}\mathrm{E}^{\rm rec}_{\gamma 2}(1-\cos\theta^{\rm rec})}$, where $\mathrm{E}^{\rm rec}_{\gamma 1}$ and $\mathrm{E}^{\rm rec}_{\gamma 2}$ are the reconstructed energies of the extended tracks ($\mathrm{E}^{\rm rec}_{\gamma 1} > \mathrm{E}^{\rm rec}_{\gamma 2}$) and $\theta^{\rm rec}$ is the reconstructed angle between the extended tracks. The MC simulation describes well the tail of the distribution, which is background-dominated. We select events with 50 MeV/c^2 $< \mathrm{M}^{\rm rec}_{\pi^0} <$ 200 MeV/c^2. The peak value is smaller than the actual π^0 mass (135 MeV) due to energy leakage of γs.

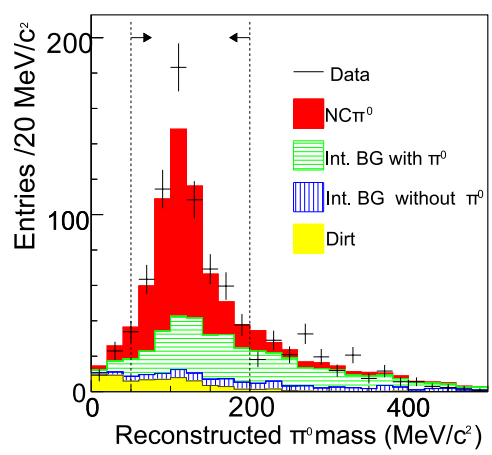

FIG. 12. The reconstructed mass of π^0s after the reconstructed vertex position cut.

8. *Event Selection Summary*

Table II shows the number of events in data and the MC at each event selection stage. The numbers for the MC simulation are normalized to the number of MRD stopped events. We select 657 events after all cuts. Subtracting the estimated background of 240 events (202 internal and 38 external) yields 417 signal events. The MC expectation is 368 events. The purity of NC π^0 production after all event selection cuts is estimated to be 61% (40% from single π production via resonance decay, 15% from coherent π production and 5% from neutrino deep inelastic scattering). According to our MC simulation, 96% of selected NCπ^0 events have one π^0 (91% from a single π^0 without any other mesons and 5% from a single π^0 with charged mesons) and 4% have two π^0s. The

efficiency for NCπ^0 production, defined as:

$$\epsilon_{NC\pi^0} = \frac{\text{the number of selected NC}\pi^0\text{ events}}{\text{the number of generated NC}\pi^0\text{ events}}, \quad (4)$$

is estimated to be 5.3%. The internal background, which accounts for 33% of this sample, contains CC π^0 production including secondary π^0s (18%), NC secondary π^0 production in detector materials (9%) and non-π^0 background (6%). According to our MC simulation, the average energy of neutrinos producing NCπ^0 events in the SciBar fiducial volume is 1.3 GeV and the average energy of neutrinos producing NCπ^0 events that pass all selection cuts is 1.1 GeV. The average energy of neutrinos producing NCπ^0s coherently is 1.1 GeV, while the average energy that pass the selection cuts is 1.0 GeV.

V. RESULTS

A. $\sigma(\text{NC}\pi^0)/\sigma(\text{CC})$ Cross Secion Ratio

We measure the ratio of the NCπ^0 production to the total CC interaction cross sections.

1. NCπ^0 Production

The efficiency corrected number of NCπ^0 events is calculated as:

$$N(\text{NC}\pi^0) = \frac{N_{\text{obs}} - N_{\text{BG}}}{\epsilon_{\text{NC}\pi^0}}, \quad (5)$$

where N_{obs} is the number of observed events, N_{BG} is the number of background events estimated by the MC simulation, and $\epsilon_{\text{NC}\pi^0}$ is the selection efficiency of NC π^0 events calculated by the MC simulation. N_{obs} and N_{BG}, $\epsilon_{\text{NC}\pi^0}$ are 657, 240.0 and 0.053, respectively. After subtracting background and correcting for the selection efficiency, the number of NCπ^0 candidates is measured to be $[7.8 \pm 0.5(\text{stat.})] \times 10^2$. For the background calculation, we use the MC expectation normalized to the number of MRD stopped events. The neutrino energy dependence of the selection efficiency for NCπ^0 events is shown in Fig. 13. The mean neutrino energy for NCπ^0 events in the sample is estimated to be 1.1 GeV after event selection cuts.

2. Total CC Interactions

The total number of CC interactions is estimated using the MRD stopped sample. The mean neutrino energy of MRD-stopped events is estimated to be 1.2 GeV. The number of CC candidates after correcting for the selection efficiency is calculated as:

$$N(\text{CC}) = \frac{N^{\text{CC}}_{\text{obs}} - N^{\text{CC}}_{\text{BG}}}{\epsilon_{\text{CC}}}, \quad (6)$$

where $N^{\text{CC}}_{\text{obs}}$ is the number of observed CC events, $N^{\text{CC}}_{\text{BG}}$ and ϵ_{CC} are the number of background events and selection efficiency in the sample, respectively, estimated with the MC simulation. We observed 21,702 MRD-stopped events (N^{CC}_{obs}). The number of background events and the selection efficiency are estimated to be 2348 ($N^{\text{CC}}_{\text{BG}}$) and 19% ($\epsilon_{\text{CC}}$), respectively. The neutrino energy dependence of the selection efficiency for CC events is shown in Fig. 14. After subtracting the background events and correcting for the efficiency, the number of CC events is measured to be $[1.02 \pm 0.01(stat.)] \times 10^5$.

3. Cross section ratio

The ratio of the NC π^0 production to the total CC cross section is measured to be:

$$\frac{\sigma(\text{NC}\pi^0)}{\sigma(\text{CC})} = \frac{N(\text{NC}\pi^0)}{N(\text{CC})} = (7.7 \pm 0.5(\text{stat.}) \pm 0.5(\text{sys.})) \times 10^{-2}, \quad (7)$$

at the mean neutrino energy of 1.14 GeV; systematic uncertainties are described in section V A 4. The MC expectation based on the Rein and Sehgal model is 6.8×10^{-2}. The total uncertainty, $\pm 0.7 \times 10^{-2}$ is obtained adding statistical and systematic uncertainties in quadrature. Although the value of this measurement is larger than the expectation by 11%, the excess corresponds to 1.3 standard deviations if the total uncertainty is taken into account.

4. Systematic errors

The sources of systematic error are divided into four categories, (i) detector response and track reconstruction, (ii) nuclear effects and neutrino interaction models, (iii) neutrino beam and (iv) dirt background. We vary these sources within their uncertainties and take the resulting change in the cross section ratio as the systematic uncertainty of the measurement. Table III summarizes the systematic errors in the NCπ^0 cross section ratio. The total systematic error is $\pm 0.5 \times 10^{-2}$ on the cross section ratio.

a. Detector response and track reconstruction The crosstalk of the MA-PMT was measured to be 3.15±0.4% for adjacent channels and is varied within the measurement error. The single photoelectron resolution of the MA-PMT is set to 50% in the simulation, to reproduce the observed dE/dx distribution of cosmic muons. The absolute error is estimated to be ±20%. Hence, we vary the single photoelectron resolution by ±20%. Birk's constant for the SciBar scintillator was measured to be 0.0208 ± 0.0023 cm/MeV [33] and is varied within the measurement error. The hit threshold for track reconstruction is varied by ±20%. A 10% difference of the total pion-carbon cross section is seen for higher energy pions

TABLE II. Event selection summary; for the MC expectation, NCπ^0signals, integral backgrounds (BG) and dirt backgrounds are shown separately. The number of CC background events is shown in parentheses.

Event selection	DATA	MC			NCπ^0	NCπ^0
		NCπ^0 signal	Internal BG (CC)	Dirt BG	Efficiency	Purity
Pre-selection Cuts	11,926	1,893	9,808 (9050)	895	27.3%	15%
Muon Track Rejection Cuts	5,609	1,377	3,785 (3326)	606	19.8%	24%
Track Disconnection Cuts	3,614	1,314	1,706 (1306)	595	18.9%	36%
Electron Catcher cut	2791	1202	1088 (714)	579	17.3%	42%
Number of Photon Tracks	973	443	389 (294)	121	6.5%	46%
π^0 Reconstructed π^0 Position Cut	905	428	382 (288)	65	6.2%	49%
Reconstructed π^0 mass	657	368	202 (140)	38	5.3%	61%

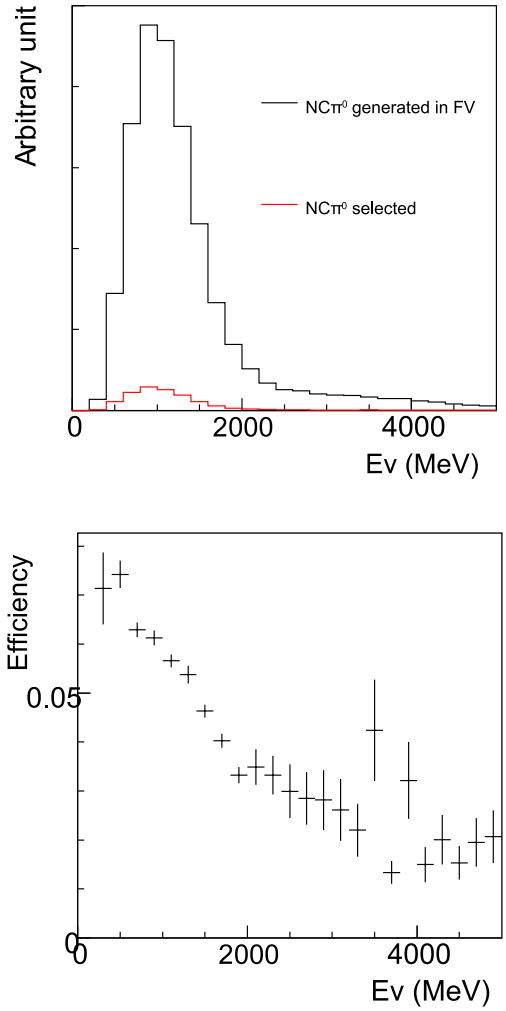

FIG. 13. Expected neutrino energy spectra and selection efficiency as a function of neutrino energy for NCπ^0 events.

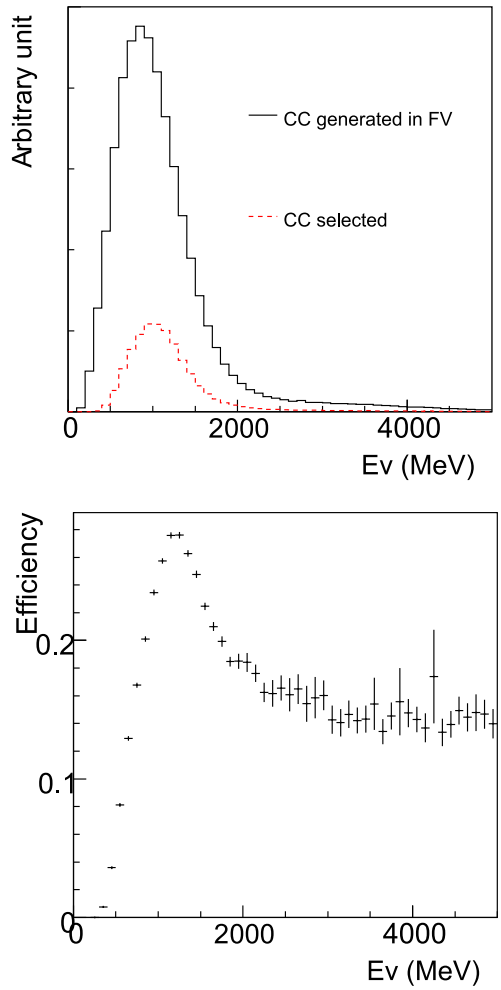

FIG. 14. Expected neutrino energy spectra and selection efficiency as a function of neutrino energy for all CC events.

TABLE III. Summary of the systematic errors in the NCπ^0 cross section ratio.

Source	error ($\times 10^{-2}$)	
Detector response	-0.39	0.38
ν interaction	-0.25	0.30
Dirt background	-0.10	0.10
ν beam	-0.11	0.22
Total	-0.48	0.54

between the GEANT4 simulation and external measurements. Hence, we vary the cross section by ±10%. The uncertainty of the energy scale of gamma rays is estimated to be ±3%. We vary the reconstructed energy of extended tracks by ±3%. For the uncertainty on reconstruction of the gamma direction, we study how the difference between data and MC distributions changes when we change the gamma direction reconstruction algorithm. We compare our standard algorithm with gamma direction reconstruction obtained using extended tracks - resulting in poorer angular resolution. We take this change as the uncertainty. The largest contribution to the uncertainty in the cross section ratio are the crosstalk of the MA-PMT (-0.00,+0.27) and the hit threshold (-0.25,+0.05).

b. Neutrino interaction models and nuclear effects The uncertainty in CC resonant pion production is estimated to be approximately ±20% based on the K2K measurement [34]. We vary the cross section of CC resonant pion production by ±20% and take that change as the systematic error. We also vary the NC/CC ratio by ±20% and take that change as a systematic error. The uncertainty in the axial vector mass for CC quasi-elastic and NC elastic scattering as well as CC(NC) resonant pion production is estimated to be approximately ±0.1 GeV/c^2 based on recent measurements [35, 36]; results from past experiments are systematically lower than recent measurements [37], and thus we only vary M_A down to 1.11 GeV/c^2, and take that change as the systematic error. The biggest contribution to the uncertainty of the cross section ratio is the CC resonant pion production (-0.14,+0.16).

We consider uncertainties in the pion interactions inside the nucleus. For pions produced by neutrino interactions, uncertainties on the cross sections for pion absorption, pion inelastic scattering and pion charge exchange in the nucleus are approximately 30% [38] in the momentum range of pions from Δ decays; we vary these pion interaction cross sections and take the resultant change in the ratio as the uncertainty. The largest contribution to the uncertainty of the cross section ratio is the pion absorption (-0.17,+0.19).

As a cross check, we measure the cross section ratio using the NUANCE event generator [30] to predict event rates and calculate efficiencies, and obtain a measured ratio of 7.9×10^{-2} (the NUANCE expectation is 7.1×10^{-2}). The result using NUANCE agrees with the NEUT result (7.7×10^{-2}) within the systematic uncertainty, so we do not add the NEUT/NUANCE difference to the systematic uncertainty.

c. Dirt Backgrounds As shown in Fig. 11, the dirt background simulation describes data at $z < -20$ cm where the dirt background is the dominant contamination. However, the statistical uncertainty is large, 15%. We scale the dirt contamination by ±15% in the final sample and take the change as the systematic error due to dirt backgrounds.

d. Neutrino Beam The uncertainties in secondary particle production cross sections in proton-beryllium interactions, hadronic interactions in the target or horn, and the horn magnetic field model are varied within their externally estimated error bands. Detailed descriptions of each uncertainty are found elsewhere [15]. Systematic uncertainties in the neutrino flux are reduced by removing the model dependent parameterization in the propagation of errors from the HARP data[15]. Uncertainties associated with the delivery of the primary proton beam to the beryllium target and the primary beam optics, which result in an overall normalization uncertainty, are not considered in this analysis since they cancel in the cross section ratio.

B. Reconstructed π^0 Kinematics

After all event selection cuts, we studied the reconstructed kinematics of the π^0s: the π^0 momentum and cosine of the π^0 angle with respect to the beam direction, as shown in Fig. 15 and Fig. 16. The NCπ^0 efficiency as functions of π^0 momentum and angle are shown in Fig. 17 and 18, respectively. The average momentum of reconstructed π^0s is estimated to be 223 MeV/c while the average momentum of true π^0s after all event selection cuts is 264 MeV/c according to our MC simulation. This difference comes from energy leakage of gamma rays. The relation between the true and reconstructed π^0 momentum is shown in Fig. 19. The momentum resolution is estimated to be 23%. The relation between the true and reconstructed π^0 direction is shown in Fig. 20. The angular resolution of π^0s is estimated to be 6°. In events with two π^0s, we choose the π^0 with the largest momentum when comparing the true and reconstructed kinematic quantities.

In the reconstructed π^0 momentum and angular distributions, we extract NCπ^0 signal events by subtracting the expected backgrounds; to estimate backgrounds, we use the MC expectation normalized to the number of MRD-stopped events. After the background subtraction, we convert the reconstructed π^0 momentum (direction) distribution to the true momentum (direction) distribution using a Bayesian unfolding method [39] using the MC simulation to define the unfolding matrix. Figure 19 (20) shows the true versus reconstructed π^0 momentum (angle) distributions; these figures are graphical represen-

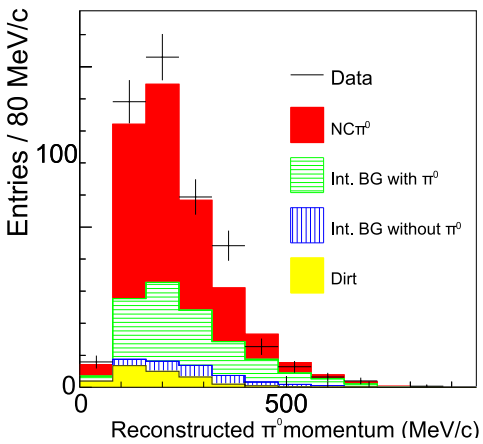

FIG. 15. The reconstructed π^0 momentum after all event selection cuts.

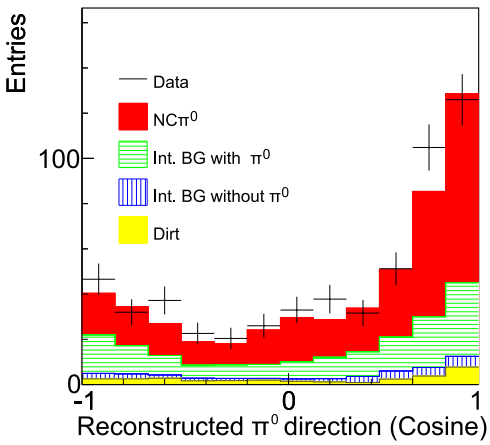

FIG. 16. Cosine of the reconstructed π^0 angle with respect to the beam direction after all event selection cuts.

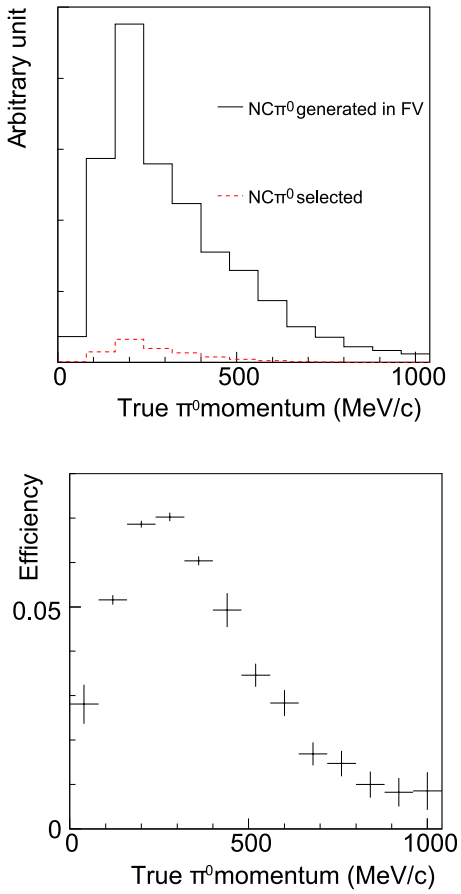

FIG. 17. The true π^0 momentum of generated MC events (solid) and selected MC events (dashed) for all NCπ^0 production processes (top), and the true π^0 momentum dependence of the efficiency of NCπ^0 production (bottom).

tations of the smearing matrices used for the unfolding. Finally, we perform the efficiency correction to obtain the true π^0 momentum (direction) distribution. Figures 21 and 22 show the π^0 momentum and direction distributions, respectively, after background subtractions, conversions to the true π^0 kinematics and efficiency corrections. To compare the shapes of the distributions, the total numbers of entries in the distributions are normalized to unity both for the measurement and the MC expectation. The shapes of these two distributions agree with the MC expectation. The systematic errors of Fig. 21 and 22 are expected to arise from the same sources, and are estimated in the same manner, as described in Sec. V A 4.

C. Coherent pion production

In the coherent pion production, the neutrino interacts the entire nucleus. In this case, the following relation should be satisfied.

$$|t| < \frac{1}{R}, \tag{8}$$

where t and R are the momentum transfer to the nucleus and the nuclear radius, respectively. Using Eq. 8, we can deduce

$$E_{\pi^0}(1 - \cos\theta_{\pi^0}) < \frac{1}{R} \sim \ 100 \text{ MeV} \tag{9}$$

according to Ref. [40]. In this equation, the E_{π^0} and θ_{π^0} are the π^0 energy and direction with respect to the neutrino beam, respectively. Hence, the fraction of coherent

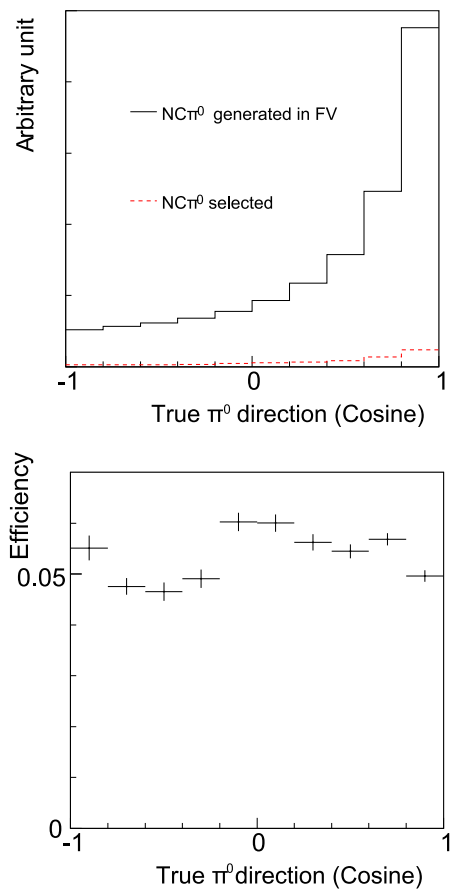

FIG. 18. The true π^0 angle with respect to the beam direction for generated MC events (solid) and selected MC events (dashed) for NCπ^0 production (top), and the efficiency for NC π^0 production as a function of the true π^0 direction (bottom).

π^0 production is extracted from the $E^{\rm rec}_{\pi^0}(1-\cos\theta^{\rm rec})$ distribution shown in Fig. 23, where $E^{\rm rec}_{\pi^0}$ is the reconstructed π^0 energy calculated as $E^{\rm rec}_{\gamma 1}+E^{\rm rec}_{\gamma 2}$. We fit this distribution using three templates made by dividing the final MC sample into NC coherent π^0, NC resonant $\pi^0$and background samples. Two parameters, $\mathrm{R_{coh}}$, $\mathrm{R_{res}}$, scale NC coherent $\pi^0$and NC resonant π^0templates independently. The scale of the background sample is fixed to unity. The expected number of events in the i-th ($i=1,2,\ldots,N(=20)$) bin in the $E^{\rm rec}_{\pi^0}(1-\cos\theta^{\rm rec})$ distribution is expressed as:

$$N_i^{\rm exp} = \mathrm{R_{coh}} \times N_i^{\rm coh} + \mathrm{R_{res}} \times N_i^{\rm res} + N_i^{\rm BG} \qquad (10)$$

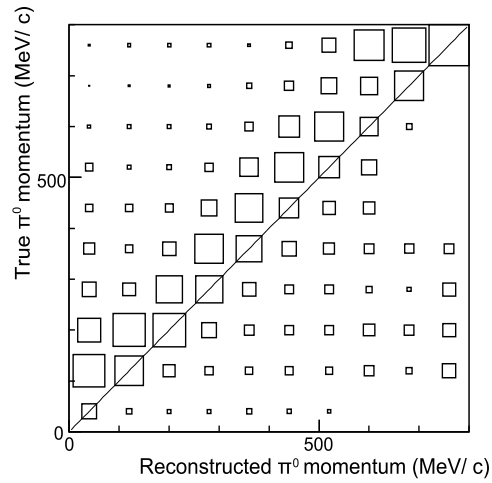

FIG. 19. The true π^0 momentum ($P^{\rm true}$) versus reconstructed π^0 momentum ($P^{\rm rec}$) from the MC simulation. The solid line shows the identity.

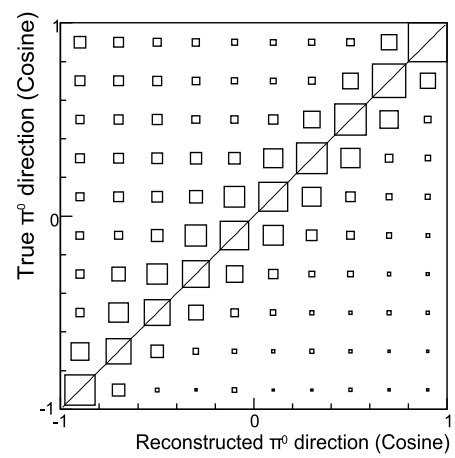

FIG. 20. The true π^0 direction ($\cos\theta^{\rm true}$) versus reconstructed π^0 direction ($\cos\theta^{\rm rec}$) from the MC simulation. The solid line shows the identity.

The fit minimizes the following χ^2:

$$\chi^2 = -2\ln\frac{f(N^{\rm obs};N^{\rm exp})}{f(N^{\rm obs};N^{\rm obs})}, \qquad (11)$$

where $N^{\rm obs(exp)}$ represents the observed (expected) number of events in all bins $(N_1^{\rm obs(exp)}, N_2^{\rm obs(exp)}, \ldots, N_N^{\rm obs(exp)})$ and $f(N^{\rm obs};N^{\rm exp})$ is the Poisson likelihood to find $N^{\rm obs}$ events when $N^{\rm exp}$ events are expected. When the systematic errors for each bin and their correlation expressed using the covariance matrix V_{jk} $(j,k=1,2,\ldots,N(=20))$ are

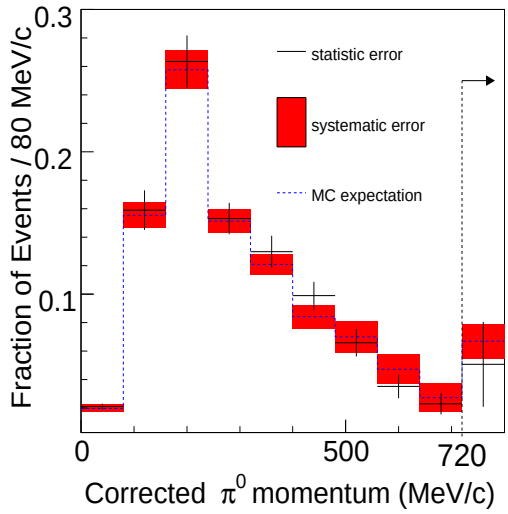

FIG. 21. The π^0 momentum distribution after all corrections described in the text, with statistical (error bars) and systematic (red boxes) uncertainties. The dashed line shows the Monte Carlo expectation based on the Rein and Sehgal model.

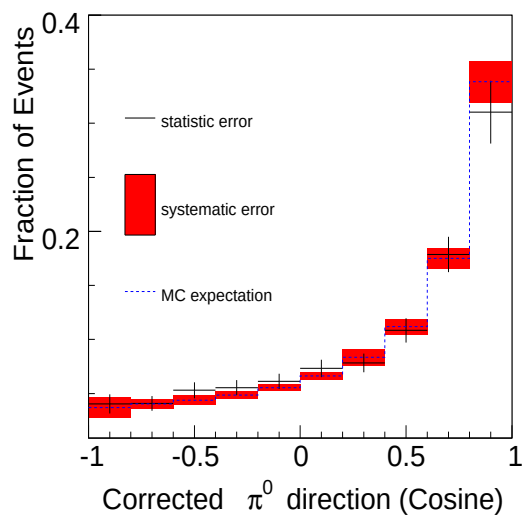

FIG. 22. The π^0 angular distribution after all corrections described in the text, with statistical (error bars) and systematic (red boxes) uncertainties. The dashed line shows the Monte Carlo expectation based on the Rein and Sehgal model.

given, the likelihood is expressed as

$$f(N^{\rm obs};N^{\rm exp};V) = A\int\Big[\Big[\prod_{i=1}^{N} dx_i \frac{{x_i}^{N_i^{\rm obs}} e^{-x_i}}{N_i^{\rm obs}!}\Big] \times \exp\Big[-\frac{1}{2}\sum_{j=1}^{N}\sum_{k=1}^{N}(x_j - N_j^{\rm exp})V_{jk}^{-1}(x_k - N_k^{\rm exp})\Big]\Big], \quad (12)$$

where A is the normalizing constant. To calculate this integral, we generate 1000 MC expectations with random variations drawn from Gaussian distributions about the expectations for each bin, with correlations, estimated from the MC simulation. Using $x_{i,m}$ for the m-th expectation in the i-th bin, the likelihood is expressed as :

$$f(N^{\rm obs};N^{\rm exp};V) = \frac{1}{M}\sum_m\prod_i \frac{x_{i,m}^{N_i^{\rm obs}} e^{-x_{i,m}}}{N_i^{\rm obs}}, \quad (13)$$

where M is the total number of random samples (1000). The result of the fit is:

$$\mathrm{R_{coh}} = 0.56 \pm 0.34, \quad (14)$$
$$\mathrm{R_{res}} = 1.33 \pm 0.16. \quad (15)$$

The $E_{\pi^0}^{\rm rec}(1-\cos\theta^{\rm rec})$ distribution after the fitting is shown in Fig. 23. The χ^2 per degree of freedom (DOF), before the fit is $17.8/20 = 0.89$, and it is $12.9/18 = 0.72$ after the fit. The statistical error and all systematic errors described in Sec. V A 4 are included in the errors of $\mathrm{R_{coh}}$ and $\mathrm{R_{res}}$. Without the systematic errors, we obtain 0.79 ± 0.30(stat.) and 1.24 ± 0.13(stat.) for $\mathrm{R_{coh}}$ and $\mathrm{R_{res}}$, respectively. The dominant systematic source is the detector response.

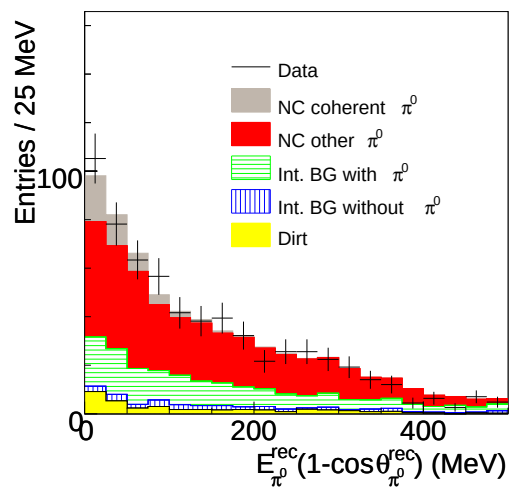

FIG. 23. $E_{\pi^0}^{\rm rec}(1-\cos\theta^{\rm rec})$ after fitting. The coherent contribution and other NCπ^0 are separately shown for the MC simulation.

The ratio of the NC coherent π^0 production to the total CC cross sections from the MC prediction based on the Rein and Sehgal model is 1.21×10^{-2}. Hence, the cross section ratios are measured to be:

$$\frac{\sigma(\mathrm{NCcoh}\pi^0)}{\sigma(\mathrm{CC})} = \mathrm{R_{coh}} \times 1.21 \times 10^{-2}, = (0.68 \pm 0.41) \times 10^{-2}, \quad (16)$$

where $\mathrm{R_{coh}}$ is 0.56±0.34. The mean neutrino energy for NC coherent π^0 events in the sample is estimated to be 1.0 GeV. This result is 1.6 standard deviations above the no coherent production assumption and consistent with the MC prediction based on the Rein and Sehgal model.

VI. CONCLUSIONS

In conclusion, we have observed the production of the NCπ^0 events by a muon neutrino beam on a polystyrene target (C_8H_8) using the SciBooNE neutrino data set of 0.99×10^{20} protons on target. The ratio of the NCπ^0 production to total CC cross sections is measured to be $(7.7 \pm 0.5(\text{stat.}) \pm 0.5(\text{sys.})) \times 10^{-2}$ at mean neutrino energy 1.1 GeV. The MC prediction based on the Rein and Sehgal model [9] is 6.8×10^{-2}. The measured shapes of the π^0 momentum and angular distributions, as shown in Figures 21 and 22 agree with the MC prediction within uncertainties. The ratio of NC coherent π^0production to the total CC cross section is measured to be $(0.7 \pm 0.4) \times 10^{-2}$ based on the Rein and Sehgal model [27], while the MC prediction is 1.21×10^{-2}.

VII. ACKNOWLEDGEMENTS

We acknowledge the Physics Department at Chonnam National University, Dongshin University, and Seoul National University for the loan of parts used in SciBar and the help in the assembly of SciBar. We wish to thank the Physics Departments at the University of Rochester and Kansas State University for the loan of Hamamatsu PMTs used in the MRD. We gratefully acknowledge support from Fermilab as well as various grants, contracts and fellowships from the MEXT and JSPS (Japan), the INFN (Italy), the Ministry of Science and Innovation and CSIC (Spain), the STFC (UK), and the DOE and NSF (USA). This work was supported by MEXT and JSPS with the Grant-in-Aid for Scientific Research A 19204026, Young Scientists S 20674004, Young Scientists B 18740145, Scientific Research on Priority Areas "New Developments of Flavor Physics", and the global COE program "The Next Generation of Physics, Spun from Universality and Emergence". The project was supported by the Japan/U.S. Cooperation Program in the field of High Energy Physics and by JSPS and NSF under the Japan-U.S. Cooperative Science Program.

[1] Y. Itow, Nucl. Phys. Proc. Suppl. **112**, 3 (2002).
[2] D. A. Harris *et al.* [MINERvA Collaboration], arXiv:hep-ex/0410005.
[3] S. J. Barish *et al.*, Phys. Rev. Lett. **33**, 448 (1974).
[4] M. Derrick *et al.*, Phys. Rev. D **23**, 569 (1981).
[5] W. Krenz *et al.* [Gargamelle Neutrino Propane Collaboration and Aachen-Brussels-CERN-Ecole Po], Nucl. Phys. B **135**, 45 (1978).
[6] W. Y. Lee *et al.*, Phys. Rev. Lett. **38**, 202 (1977).
[7] P. J. Nienaber, Ph.D. thesis, University of Illinois at Urbana-Champaign, 1988.
[8] S. Nakayama *et al.* [K2K Collaboration], Phys. Lett. B **619**, 255 (2005) [arXiv:hep-ex/0408134].
[9] D. Rein and L. M. Sehgal, Annals Phys. **133**, 79 (1981).
[10] A. A. Aguilar-Arevalo *et al.* [MiniBooNE Collaboration], Phys. Lett. B **664**, 41 (2008) [arXiv:0803.3423 [hep-ex]].
[11] M. Hasegawa *et al.* [K2K Collaboration], Phys. Rev. Lett. **95**, 252301 (2005) [arXiv:hep-ex/0506008].
[12] K. Hiraide *et al.* [SciBooNE Collaboration] Phys. Rev. D **78**, 112004 (2008).
[13] K. Hiraide *et al.* [SciBooNE Collaboration] Proceedings of NuInt09 (2009), arXiv:0909.5127v1[hep-ex].
[14] H.-K. Tanaka *et al.* [SciBooNE Collaboration] Proceedings of NuInt09 (2009), arXiv:0910.4754[hep-ex].
[15] A. A. Aguilar-Arevalo *et al.* [MiniBooNE Collaboration], Phys. Rev. D **79**, 072002 (2009) arXiv:0806.1449 [hep-ex].
[16] K. Nitta *et al.*, Nucl. Instrum. Meth. A **535** (2004) 147 [arXiv:hep-ex/0406023].
[17] M. Yoshida *et al.*, IEEE Trans. Nucl. Sci. **51** (2004) 3043.
[18] S. Buontempo *et al.*, Nucl. Instrum. Meth. A **349** (1994) 70.
[19] M. G. Catanesi *et al.*, Eur. Phys. J. C **52**, 29 (2007) [arXiv:hep-ex/0702024].
[20] I. Chemakin *et al.* [E910 Collaboration], Phys. Rev. C **77**, 015209 (2008) [Erratum-ibid. C **77**, 049903 (2008)] [arXiv:0707.2375 [nucl-ex]].
[21] Y. Hayato, Nucl. Phys. Proc. Suppl. **112**, 171 (2002).
[22] G. Mitsuka, AIP Conf. Proc. **981**, 262 (2008).
[23] R. A. Smith and E. J. Moniz, Nucl. Phys. B **43**, 605 (1972) [Erratum-ibid. B **101**, 547 (1975)].
[24] S. K. Singh, M. J. Vicente-Vacas, and E. Oset, Phys. Lett. B **416**, 23 (1998) [Erratum-ibid. B **423**, 428 (1998)].
[25] D. Rein, Z. Phys. C **35**, 43 (1987).
[26] L. L. Salcedo, E. Oset, M. J. Vicente-Vacas, and C. Garcia-Recio, Nucl. Phys. A **484**, 557 (1988).
[27] D. Rein and L. M. Sehgal, Nucl. Phys. B **223**, 29 (1983).
[28] D. Rein and L. M. Sehgal, Phys. Lett. B **657**, 207 (2007) [arXiv:hep-ph/0606185].
[29] M. Gluck, E. Reya, and A. Vogt, Eur. Phys. J. C **5**, 461 (1998) [arXiv:hep-ph/9806404].
[30] D. Casper, Nucl. Phys. Proc. Suppl. **112**, 161 (2002) [arXiv:hep-ph/0208030].
[31] A. Heikkinen, N. Stepanov, and J. P. Wellisch, *In the Proceedings of 2003 Conference for Computing in High-Energy and Nuclear Physics (CHEP 03), La Jolla, California, 24-28 Mar 2003, pp MOMT008* [arXiv:nucl-th/0306008].
[32] H. Maesaka, Ph.D. thesis, Kyoto University, 2005.
[33] M. Hasegawa, Ph.D. thesis, Kyoto University, 2006.
[34] A. Rodriguez *et al.* [K2K Collaboration], Phys. Rev. D **78**, 032003 (2008) [arXiv:0805.0186 [hep-ex]].
[35] R. Gran *et al.* [K2K Collaboration], Phys. Rev. D **74**, 052002 (2006) [arXiv:hep-ex/0603034].
[36] A. A. Aguilar-Arevalo *et al.* [MiniBooNE Collaboration], Phys. Rev. Lett. **100**, 032301 (2008) [arXiv:0706.0926 [hep-ex]].
[37] V. Bernard, L. Elouadrhiri, and U. G. Meissner, J. Phys. G **28**, R1 (2002) [arXiv:hep-ph/0107088].

[38] D. Ashery, I. Navon, G. Azuelos, H. K. Walter, H. J. Pfeiffer, and F. W. Schleputz, Phys. Rev. C **23**, 2173 (1981).

[39] G. D'Agostini, Nucl. Instrum. Meth. A **362**, 487 (1995).

[40] K. S. Lackner, Nucl. Phys. B **153**, 526 (1979).